SUPPLEMENTARY INFORMATION
Probing optical excitations in chevron-like armchair graphene nanoribbons

(Dated: August 18, 2017)

PACS numbers:

I. RDS MEASUREMENTS

A. RDS data

Figure 1 shows the full information, i.e. the real and the imaginary parts of the RD spectra recorded during the ch-AGNR growth.

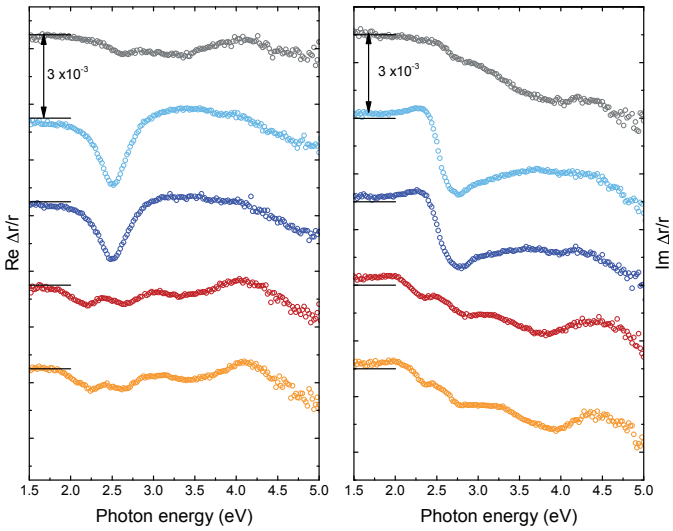

FIG. 1: Real part (left) and imaginary part (right) of the RD spectra recorded at different stages of ch-AGNR growth: pristine Au(778) surface at 200°C (grey circles), intermediate oligomer phase at 200°C (light blue circles) and 250°C (dark blue circles), ch-AGNR at 420°C (red circles) and after cooling to 200°C (orange circles). The spectra are vertically shifted in increments of -3×10^{-3} for better viewing.

B. Three-phase model analysis

Since small differences in the RD signals, e.g. due to different temperatures, and uncertainties in the Au dielectric function used to extract $\Delta\epsilon$ from Eq. (1) (main text) could influence the final results, the data analysis was crosschecked by: (a) subtracting different RD spectra of Au(788) (recorded at 150°C and 200°C, respectively); (b) using three different dielectric functions for Au [ϵ_b in Eq. (2)]. The different ϵ_b to model the gold substrate are (*i*) au_2 of WVASE32 database by J.A. Wollam Co., Inc (used already for the N7-AGNR fitting in Ref.[1]); (*ii*) Au single crystal data from Ref.[2]; (*iii*) a dielectric function determined via variable angle spectroscopic ellipsometry (in air) from a 7AGNR/Au(788) sample. Note that for

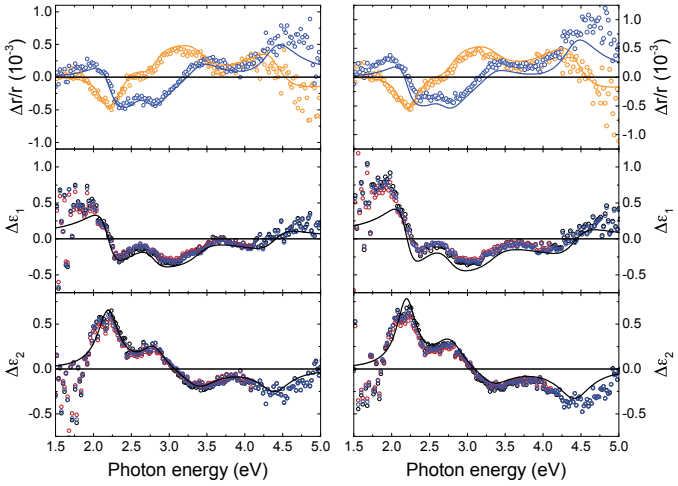

FIG. 2: Top row: Real and imaginary part of the RD spectra from ch-AGNR recorded at 200°C (orange and blue circles respectively) after subtraction of the RD spectra of the pristine Au(788) surface measured at 150°C (left column) and 200°C (right column), respectively. The middle and lower rows show the calculated $\Delta\epsilon_1$ and $\Delta\epsilon_2$ [Eq. (2)] using three different gold dielectric functions for ϵ_b. (*i*) (black circles), (*ii*) (red circles) and (*iii*) (blue circles). The black solid lines are the fit to a Lorentzian oscillator model including 4 transitions and using the dielectric function (*i*). The solid lines in the top panels show the real (orange line) and imaginary (blue line) part of the RD spectra calculated from the fitted $\Delta\epsilon$ (black lines), respectively.

(*iii*) the error due to the GNRs should be negligible.

As shown for ch-AGNRs in Fig. 2, the subtraction of the different Au(788) spectra does not change the characteristic shape of the $\Delta\epsilon$ spectra (left vs. right panels). Likewise, use of the different functions for ϵ_b has almost no effect at all (symbols with different colors in the lower two panels). In summary, we find that all the different options listed above have practically no influence on the determination of $\Delta\epsilon$ and the main transition energies, whereas they have a minor influence on the exact widths and amplitudes of the Lorentzian oscillators in the fits of $\Delta\epsilon$ using Eq. (1). For these reasons, we chose to subtract the substrate signal as recorded at 150°C and to use the same ϵ_b (*i*) as used in Ref.[1], in all the calculations presented in this paper.

We want to note that the shape of the first peak of $\Delta\epsilon_2$ in Fig. 2 suggests a possible superposition of two transitions. Indeed, we find that $\Delta\epsilon$ can be described quite well by 5 Lorentzian oscillators (Figure 3), namely by adding an extra transition for light polarized along the ribbon axis (x) at 2.05 eV. As a consequence, the transition at

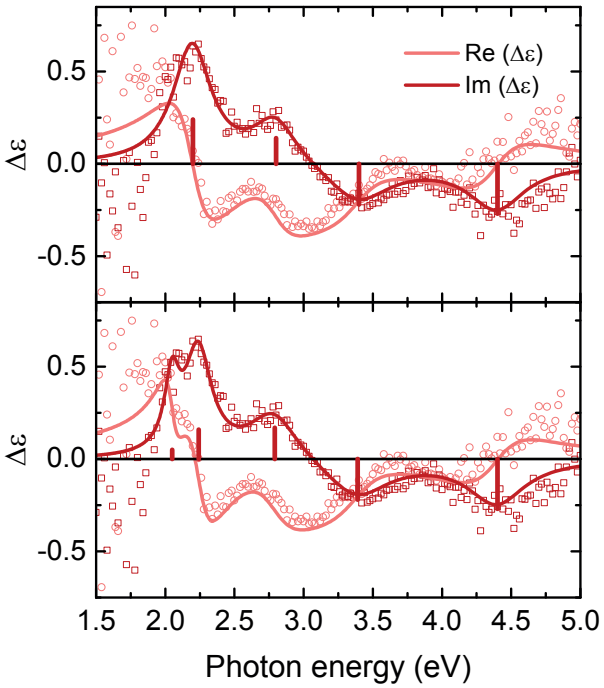

FIG. 3: Dielectric functions of ch-AGNR extracted from the RDS data according to Eq. (2) (symbols) and fitted to a Lorentzian oscillator model (lines) using four (top panel) and five (bottom panel) Lorentzian oscillator transitions. Positions and intensities of the fitted Lorentzian oscillator transitions are shown as vertical bars.

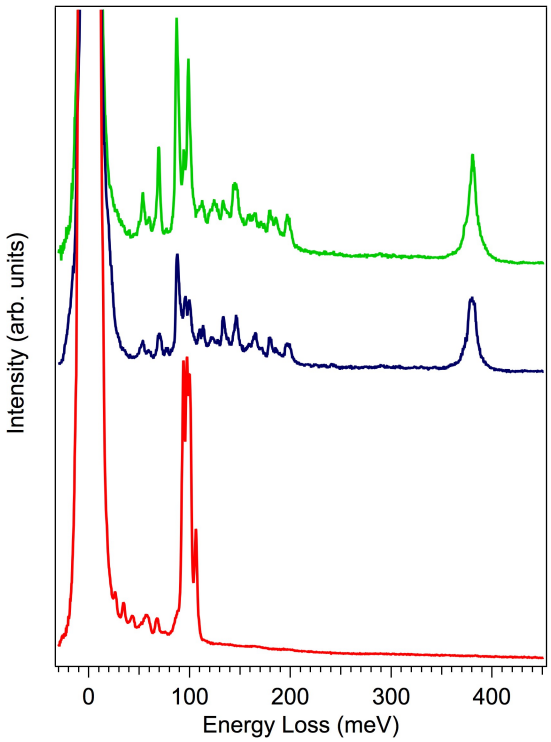

FIG. 4: Vibrational HREEL spectra of the monomer (green), polymer (blue) and ch-GNR (red). For the sake of clarity, monomer and polymer spectra are vertically shifted.

2.20 eV is slightly shifted to 2.24 eV, whereas the higher energy transitions are almost not affected. Since, however, this fit is not as robust as for the model including only four Lorentzian oscillators, we decided to use the latter.

II. HREELS MEASUREMENTS

A. Monitoring the growth process

The vibrational HREEL spectra corresponding to the different steps of ch-AGNR formation are reported in Fig. 4. For both the monomer and the polymer phase, spectra are characterized by the CH out-of-plane vibration manifold $\gamma(CH)$, in the 80-110 meV region, and the CH in-plane manifold $\delta(CH)$ in the 110-200 meV region; moreover, the intense peak associated with the CH stretching mode $\nu(CH)$ is observed at 375 meV. The observed intensity of the in-plane modes $\delta(CH)$ and $\nu(CH)$ is a clear indication of the non-planarity of the adsorbed moieties. After annealing to 450°C, the intensity of the $\nu(CH)$ and $\delta(CH)$ modes is totally quenched, while that of the $\gamma(CH)$ manifold greatly increases. In agreement with previous findings[3], these changes clearly prove the evolution of the adsorbed moieties into a planar species which lay flat on the surface, i.e. the formation of dehydrogenated ch-AGNR. As far as the polymer phase is concerned, comparison between the HREEL spectra of the monomer and polymer phase does not provide a clear fingerprint of its formation. Therefore, following the literature[4,5], we considered the occurence of Br desorption from the surface at 250° C, as observed in XPS spectra (not shown), as the indication of polymer formation.

B. EEL spectra at different primary beam energy

EELS spectra taken in the electronic excitation region, could provide important information of the optical and electronic properties of the adsorbed species. To this aim, the contribution to EEL spectra of the gold surface plasmon excitation (Au-SP, laying at 2.6 eV) should be carefully taken into account. Indeed, as reported in literature[6], the Au-SP intensity strongly increases with the primary beam energy. In Fig. 5 the clean surface and ch-AGNR EEL spectra are reported and compared for different primary beam energies, i.e. 9 eV and 20 eV. Quite clearly, the spectra taken at E_p=20 eV are dominated by the gold SP feature, the clean and the ch-AGNR spectra displaying quite subtle differences. On the other hand, for E_p=9 eV, the contribution of the Au-SP strongly decreases and the GNR features become dominant. All EEL spectra have been therefore taken at

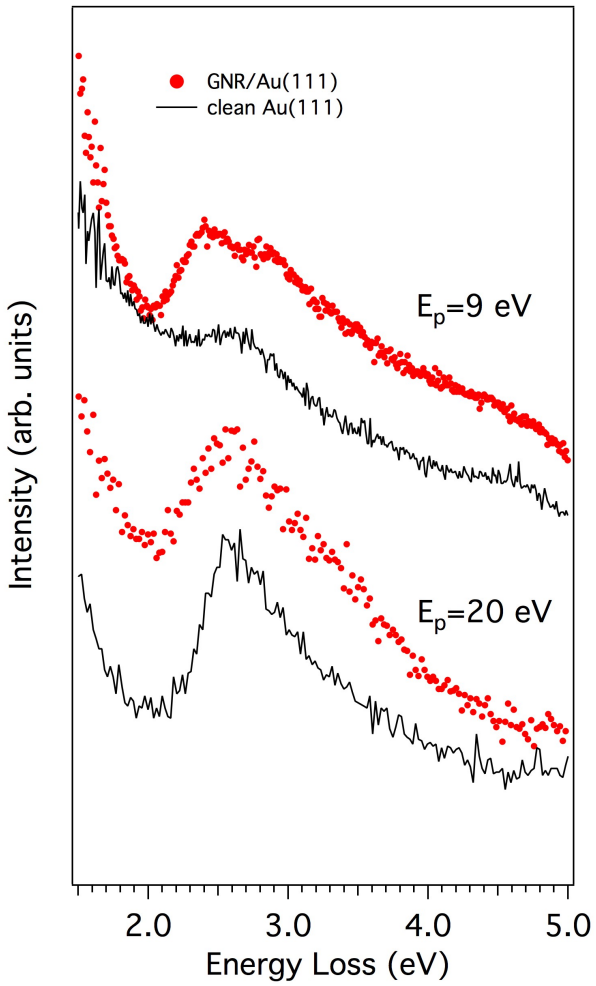

FIG. 5: EEL spectra of the clean Au(111) surface (black solid line) and ch-AGNR/Au(111 (red circles), taken at $E_p = 9$ eV (upper curves) and $E_p = 20$ eV. The $E_p = 9$ eV curves are upward shifted for convenience.

E_p=9 eV, and the Au substrate contribution has been carefully taken into account, exploiting the 3PM.

C. EELS Three-phase model analysis

According to EELS theory[7], EELS spectra can be calculated as the product of the kinematic factor and the system loss function. The kinematic factor was evaluated from the experimental scattering condition (i.e. primary beam energy E_p, scattering angles θ_i, θ_o), integrating over the analyzer angular acceptance[8]. The system loss function, given by Eqs. (3-5) (main text), was obtained using as input the substrate dielectric function and a model adsorbate dielectric function, built up by N Lorentzian oscillators. The intensity, energy and damping of the Lorentzian oscillators are used as fitting parameters to reproduce the experimental data.

As a first step in the fitting procedure, we checked

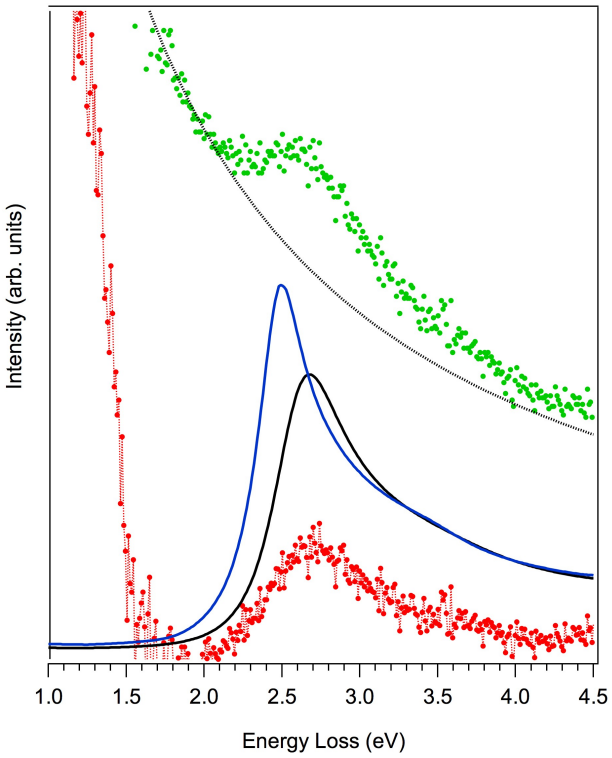

FIG. 6: EEL spectrum of the Au(111) clean surface taken at $E_p = 9$ eV, prior (green symbols) and after (red symbols) background subtraction (dotted black line). The EEL spectrum calculated using the same gold dielectric function of the RDS analysis is reported as blue curve; the black curve correposponds to the EEL spectrum calculated using the empirically modified gold dielectric function

the validity of our model for the case of the clean gold substrate. In Fig. 6, the clean Au(111) EEL spectrum, taken at $E_p = 9$ eV, is reported prior and after exponential background subtraction, and compared to the calculated EELS (blue solid line), obtained using the same gold dielectric function of the RDS analysis (i.e. au_2 of WVASE32 database by J.A. Wollam Co., Inc).

The obtained agreement is fair, but the calculated spectrum is narrower than the experimental one, and slightly shifted to lower energies. This discrepancies are due to the fact that EELS probes $\epsilon_b(\omega, \mathbf{q})$, i.e the dielectric function for finite values of the momentum transfer $\mathbf{q}$) while the dielectric function taken from the literature, which is derived from optical measurements, corresponds to $\epsilon_b(\omega, \mathbf{q} \to 0)$. A much better agreement (black line) with the experimental spectrum was obtained by a small modification of $\epsilon_b(\omega, 0)$, i.e. a shift to higher energies by 0.13 eV and a modest broadening. This modified dielectric function represents a quite fair empirical estimate of $\epsilon_b(\omega, \mathbf{q})$, and has therefore been used in the 3PM analysis of the polymer and ch-AGNR EEL spectra.

[1] R. Denk, M. Hohage, P. Zeppenfeld, J. Cai, C. A. Pignedoli, H. Söde, R. Fasel, X. Feng, K. Müllen, S. Wang, et al., Nat. Commun. **5**, 4253 (2014).
[2] R. L. Olmon, B. Slovick, T. W. Johnson, D. Shelton, S.-H. Oh, G. D. Boreman, and M. B. Raschke, Phys. Rev. B **86**, 235147 (2012).
[3] C. Bronner, S. Stremlau, M. Gille, F. Brauße, A. Haase, S. Hecht, and P. Tegeder, Angew. Chem. Int. Edit. **52**, 4422 (2013).
[4] J. Cai, P. Ruffieux, R. Jaafar, M. Bieri, T. Braun, S. Blankenburg, M. Muoth, A. P. Seitsonen, M. Saleh, X. Feng, et al., Nature **466**, 470 (2010).
[5] A. Batra, D. Cvetko, G. Kladnik, O. Adak, C. Cardoso, A. Ferretti, D. Prezzi, E. Molinari, A. Morgante, and L. Venkataraman, Chem. Sci. **5**, 4419 (2014), ISSN 2041-6520, URL <GotoISI>://WOS:000343004300038.
[6] L. Vattuone, M. Smerieri, T. Langer, C. Tegenkamp, H. Pfnür, V. Silkin, E. V. Chulkov, P. M. Echenique, and M. Rocca, Phys. Rev. Lett. **110**, 127405 (2013).
[7] H. Ibach and D. L. Mills, *Electron energy loss spectroscopy and surface vibrations* (Academic press, 1982).
[8] H. Ibach, *Electron energy loss spectrometers* (Springer, 1991).